Optical Materials 120 (2021) 111428

Contents lists available at ScienceDirect

Optical Materials

journal homepage: www.elsevier.com/locate/optmat

Research Article

Random lasing at localization induced in correlated colloidal system

Christian Tolentino Dominguez [a], Anderson A.V. Gomes [a], Niklaus U. Wetter [b], Jessica Dipold [b], Valdeci Mestre [c], Weliton S. Martins [d], Ernesto Jiménez-Villar [a,*]

[a] Departamento de Física, Universidade Federal da Paraíba, Joao Pessoa, PB, 58051-970, Brazil
[b] Instituto de Pesquisas Energéticas e Nucleares, CNEN-IPEN, São Paulo, 05508-000, Brazil
[c] CCEA, Universidade Estadual da Paraíba, Patos, PB, 58706-560, Brazil
[d] Programa de Pós-Graduação Em Engenharia Física, Unidade Acadêmica Do Cabo de Santo Agostinho, Universidade Federal Rural de Pernambuco, Cabo de Santo Agostinho, PE, 54518-430, Brazil

ARTICLE INFO

Keywords:
Localization of light
Random laser
Scattering media
Correlation-induced localization

ABSTRACT

Random lasers have the potential for cheap and coherent light sources which, in the particular case of colloidal suspensions, are completely flexible and can take on any desired shape. Here, we studied random lasing in correlated colloidal systems composed by TiO_2@Silica nanoparticles suspended in ethanol solutions of Rhodamine 6G. TiO_2 particles with two different silica layers (thicknesses of 40 nm and 70 nm) were prepared. The Random laser performance improves when the silica shell is thicker (70 nm), which was attributed to a stronger localization of light (higher density of localized states) induced by stronger correlation in the scatterers' (TiO_2@Silica) position as a consequence of a stronger and longer-range Coulomb interaction between the scatterers. Light diffraction patterns in both TiO_2@Silica suspensions showed a stronger correlation in the scatterers' position, being stronger when the silica shell is thicker.

1. Introduction

Core-shell TiO_2@Silica nanoparticles (NPs) show suitable properties for bio-photonics applications as UV and UVB absorbers [1] and in photocatalytic degradation of dyes and drugs [2]. In particular, core-shell TiO_2@Silica NPs have been introduced as scattering medium for localization of light [3] [–] [5] and random laser (RL) [6–10]. In this work, random lasing is studied in a scattering medium containing core-shell TiO_2@Silica NPs. Random lasers (RLs) present a major advantage over regular lasers as the required technology for their production is relatively simple. RLs can be produced in several different forms such as1D fiber random lasers [11], 2D flexible and wavelength-tunable random laser [12], and 3D random laser with directional output beam [13]. Here, we studied the colloidal structure and random laser action in a scattering medium composed by core-shell TiO_2@Silica NPs, with two different silica layers (thicknesses of 40 nm and 70 nm), suspended in a Rhodamine 6G (R6G) ethanol solution. The silica shell on TiO_2 core (rutile, 410 nm mean diameter) induces an electrostatic field on the TiO_2@Silica NPs surface, which gives rise to strong Coulomb interaction as [TiO_2@Silica] is increased [14]. Additionally, the silica shell provides optical colloidal stability (OCS) [15], light-coupling enhancement with the TiO_2 scatterer cores [16] and inertness (lower dye photodegradation) [6,15,16], which have enabled their use in numerous other applications [17–21]. In our recent work [14], we showed that the correlation in the scatterers' position (TiO_2@Silica NPs), due to the long-range Coulomb interaction, favors significantly photon interference (localization) [22–24], which induces an enhancement of light-matter coupling (enhanced absorption and Raman signal strength) [3–5,14,25,26]. Localization of light gives rise to other associated phenomena, such as, a photon-molecule bound state [27,28], which in turn, leads to the suppression of vibrational relaxation and spontaneous emission [29]. Several works that have claimed the observation of localization of light [30] [–] [32], were initially questioned [33,34] and later refuted by their authors [35,36]. The strategy used in these previous works was to increase the scattering strength by increasing the scatterers' concentration (randomly distributed scatterers) in order to reach the Ioffe-Regel criterion ($kl_T \sim 1$), where $k = 2\pi/\lambda$ and l_T are the wave number and transport mean free path, respectively. However, the increase of the scatterers concentration decreases the separation between them and favors the near field coupling, which can hamper localization of light [37]. Recently, Kravtsov and co-workers showed the universality of the localization phenomenon at

* Corresponding author.
E-mail address: Ernesto.Jimenez@uv.es (E. Jiménez-Villar).

https://doi.org/10.1016/j.optmat.2021.111428
Received 2 May 2021; Accepted 27 July 2021
Available online 3 August 2021

correlated long-range hopping in higher dimensional systems (*correlation-induced localization*) [22]. Dal Negro and co-workers predicted also theoretically that aperiodic correlations incorporated during the engineering of photonic media (e.g. metallic nanostructures) are suitable photonic platforms for localization of light, revealing strongly enhanced light-matter coupling compared to the traditional periodic and homogeneous random media [23,24]. The long-range Coulomb interaction between scatterers (longer range than the mean separation between scatterers) increases with the thickness of the electric double layers on TiO_2@Silica NPs [38,39]. The theoretical framework employed in colloid science to study particle-particle interactions has been the classical theory of Derjaguin-Laudau-Verwey-Overbeck (DLVO) [38]. This theory is based on the idea that pair-wise interactions arise from the interplay of attractive van der Waals forces (F_{attr}) and repulsive Coulomb forces (F_{rep}, double layer force) screened by the Debye-Hückel ions cloud. Depending on the particle size and the thickness of the double layer, the electrostatic repulsion potential (U_{elec}) between two colloidal particles of radii a and a negligible Stern layer thickness can be expressed as:

$\mathbf{U_{elec}}(\boldsymbol{r}) = 2\boldsymbol{\pi}\boldsymbol{\varepsilon}_0\boldsymbol{\varepsilon}_\mathbf{r}(\boldsymbol{a}+\boldsymbol{\Delta})\boldsymbol{\psi}_0{}^2\boldsymbol{e}^{[-\boldsymbol{\kappa}(r-2a)]}$ where ε_r is the permittivity of the medium, ψ_0 is the potential at the particle surface, which can be estimated from the ζ-potential measurements [40] and κ is the inverse Debye length (λ_{Debye}), which is the thickness of the double layer. For spherical particles and constant surface potential and the background ionic strength, the van der Waals attraction, U_{vdw}, between the two particles can be calculated as:

$\mathbf{U_{vdw}}(\boldsymbol{r}) = -\frac{A}{6}\left[\frac{2a^2}{r^2-4a^2}+\frac{2a^2}{r^2}+\ln\frac{r^2-4a^2}{r^2}\right]$ where A is the Hamaker constant. Note that the modulus of both potentials (U_{elec} and U_{vdw}) increases when the radii a of the particles increases, which induces a stronger interaction between them. The thickness of the double layer (λ_{Debye}) can be determined by the measurement of the hydrodynamic diameter, D_{Hyd}, $\left(\boldsymbol{\lambda_{Debye}} \approx \frac{\mathbf{D_{Hyd}}}{2} - \boldsymbol{a}\right)$. When the mean separation distance between particles (r_m) is similar or smaller than D_{hyd}, strong particle interaction is expected, which leads to a correlation in the particles' position [14,41]. This means that when λ_{Debye} is of the order of or larger than $h_m/2$, where h_m is the mean distance between the opposite particle surfaces, a sharp secondary minimum of the potential is expected. The crystallization starts when the colloidal particles fall into this secondary minimum of depth larger than the thermal energy. Note that an increase of the silica shell thickness would lead to an increase of particle radii a and λ_{Debye}, which would induce a stronger interaction between TiO_2@Silica NPs favoring the correlation in the scatterers' position (colloidal crystallization). The latter has been pointed out in our recent work [14], in which it was proposed to study TiO_2@Silica suspensions with thicker silica shell. In this work [14], localization of light and associated phenomena were studied for a broad range of concentrations [TiO_2@Silica NPs], using SST of ~40 nm. In other previous works [7,8], random lasing was also studied in the same TiO_2@Silica suspension (SST~40 nm), observing narrow peaks arising in the RL emission spectrum for collection from a small micrometric volume. This kind of peaks or spikes have also been observed over a broad range of scattering strengths [42], and have been associated by Stone, Zaitsev and co-workers [43,44] to effective cavities in the system (both for diffusive or localization regimes) and not to coherent feedback lasing by localization, as originally thought. In the present work, we focus on a comparative study of random lasing and transport of light performed for TiO_2@Silica suspensions with two different SST of ~40 nm & ~70 nm. Additionally, for these two latter colloidal systems, the correlation in the scatterers' position (colloidal crystallization) is studied by light diffraction patterns obtained in the backscattering configuration. The hydrodynamic diameter (D_{Hyd}) of the TiO_2@Silica NPs, measured by dynamic light scattering (DLS) at very low [TiO_2@Silica], shows a larger D_{Hyd}~1450 nm (λ_{Debye} ~450 nm) for the thicker silica shell (TiO_2@SiO_2–SiO_2) when compared to D_{Hyd}~890 nm (λ_{Debye} ~200 nm) for the thinner silica shell (TiO_2@SiO_2). Light diffraction patterns, collected in the backscattering configuration, show stronger correlation in the scatterers' position for the TiO_2@SiO_2–SiO_2 system (thicker silica shell) when compared to the TiO_2@SiO_2 system (thinner silica shell). Light transmitted by the TiO_2@SiO_2–SiO_2 system is lower than the TiO_2@SiO_2. For the TiO_2@-SiO_2–SiO_2 system, RL efficiency is higher than for TiO_2@SiO_2. We attribute these results to a stronger localization of light (higher density of localized states) in the TiO_2@SiO_2–SiO_2 system, which is induced by stronger correlation of the scatterers' positions as consequence of the longer-range Coulomb interaction between TiO_2@SiO_2–SiO_2 NPs (larger λ_{Debye}).

2. Material and methods

2.1. Synthesis of the TiO_2@SiO_2 and TiO_2@SiO_2–SiO_2 NPs

The TiO_2@SiO_2–SiO_2 NPs were synthetized in two stages. First, TiO_2 NPs (Dupont, Inc. R900) with an average diameter of 410 nm and 25 % polydispersity were coated with a silica shell of ~40 nm (TiO_2@SiO_2) via the Stöber method [3,45]. In the second stage, the previous synthesis procedure was repeated with the TiO_2@SiO_2 NPs previously synthetized obtaining a thicker silica shell ~70 nm (TiO_2@SiO_2–SiO_2). Briefly, 5 g of TiO_2 NPs were dispersed in 500 mL of spectroscopic ethanol (MERCK). This suspension was submitted to an ultrasound bath for 30 min to disperse the particles. Next, while constantly stirring the suspension, 10 mL of TEOS (sigma Aldrich Inc.) and 6.67 mL of ammonia P.A. (NH4OH 28%–30 % MERCK) were added alternately in volumes of 100 μl and 220 μl, respectively. The suspension of synthesized TiO_2@Silica NPs was rota-evaporated and dried in an oven at 70 °C for 2 h.

2.2. Characterization

Images obtained by transmission electron microscopy (TEM) of the TiO_2@SiO_2–SiO_2 NPs (Fig. 1) show a silica shell of around 70 nm thickness. Pure silica NPs of ~40–50 nm diameter are also observed.

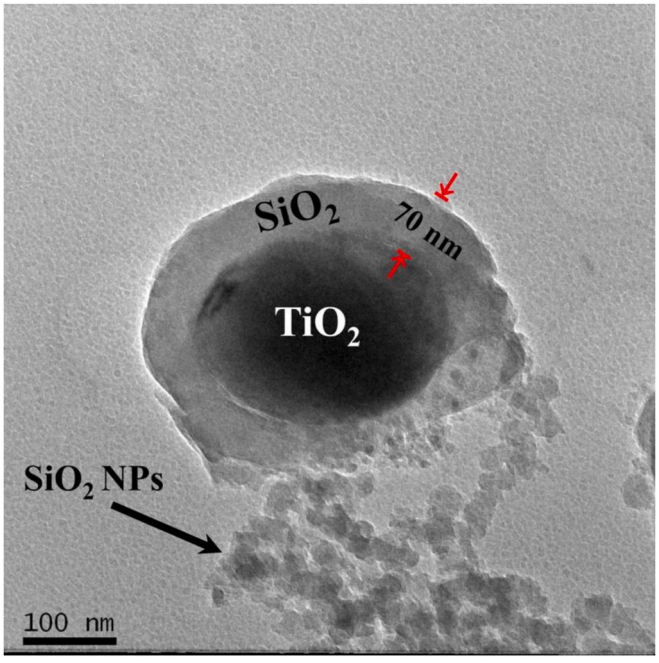

Fig. 1. TEM image of the core–shell TiO_2@SiO_2–SiO_2 NPs. The image shows the presence of silica (light gray) on top of the TiO_2 NPs (darker). The black arrow indicates the isolated silica NPs also synthesized during TEOS hydrolysis. The red arrows indicate a silica shell of around 70 nm thickness.

TEM was performed on a Jeol 200 kV transmission electron microscope, model JEM-2100. The commercial carbon-coated Cu TEM grid was immersed in the TiO_2@SiO_2–SiO_2 suspension that had previously been diluted 1000-fold and then left to dry, before being introduced into the microscope. TEM images of TiO_2@SiO_2 NPs can be found in a previous work [3]. The stoichiometric ratio (Ti/Si) of the TiO_2@SiO_2 and TiO_2@SiO_2–SiO_2 NPs was determined by energy dispersive X-ray fluorescence (ED-XRF). For ED-XRF characterization, 200 mg of dried sample powder (TiO_2@SiO_2 & TiO_2@SiO_2–SiO_2) were pressed into a pellet with 12 mm diameter. The hydrodynamic diameter (D_{Hyd}) of the TiO_2@SiO_2 and TiO_2@SiO_2–SiO_2 NPs suspended in ethanol, which gives an estimative of the extension range of the Coulomb interaction, was determined by dynamic light scattering (DLS) at very low [NPs]. A Horiba, model Nano Partica SZ-100 was used to measure D_{Hyd}.

2.3. Random laser samples preparation and experimental setup

Two RL laser samples were prepared by dispersing of the TiO_2@SiO_2 and TiO_2@SiO_2–SiO_2 NPs in ethanol solution of R6G. The TiO_2@SiO_2 and TiO_2@SiO_2–SiO_2 NPs at [$140x10^{10}$ NPs mL^{-1}], which correspond to filling fractions (*FF*) of TiO_2 (rutile) of 4.8 %, were dispersed in ethanol solution and R6G at [10^{-4} M] was added to both suspensions. We remark that in a previous work [7], a detailed random lasing study was performed in the same TiO_2@SiO_2 suspension (*FF* = 4.8 %). Additionally, we highlight that in our recently published work [14], for TiO_2@SiO_2 suspension at this *FF* = 4.8 %, a strongly enhanced light-matter coupling and strong correlation in the scatterers' positions have been observed. However, for TiO_2@SiO_2 suspensions with *FF*<1 %, no enhancement of light-matter coupling nor correlation in the scatterers' positions were observed. To perform the RL study, 400 μL of each sample was put in quartz cuvettes of 2 mm optical pathway. The samples were pumped by the second harmonic of a Q-switched Nd:YAG (Continuum Minilite II, 25 mJ, 532 nm, with a pulse width of ~4 ns) at repetition rate of 10 Hz and with a spot size of ~1.8 mm. The emission spectra were collected through a multimode optical fiber (200 μm), coupled to a spectrometer HR4000 UV−VIS (Ocean Optics), with a 0.17 nm spectral resolution (FWHM). The pumping energy fluence per pulse was varied between 0.01 and 160 mJ cm^{-2}. The schematic diagram of the experimental setup for RL studies can be found in the supplementary materials (Fig. S1a).

2.4. Transmission experiment

For both TiO_2@SiO_2 and TiO_2@SiO_2–SiO_2 NPs systems with *FF* = 4.8 % and R6G at [10^{-4} M], the intensity profile *I*(x,y) of a probe beam (linearly polarized He–Ne laser) was measured after propagating a distance of $d \approx 1.8$ mm through the samples. A CCD camera collected the image of the photon cloud at the sample's output face. In order to obtain a meaningful statistic, a total of 10 intensity profiles, collected for different input points and collection times, were recorded for each sample. The diameter of the input probe beam was <50 μm full-width at half-maximum (FWHM). The experimental setup for the transmission experiment can be found in our recently published work [14].

2.5. Light diffraction from backscattered light

A linearly polarized laser beam (He–Ne) was used to measure light diffracted by the TiO_2@SiO_2 and TiO_2@SiO_2–SiO_2 systems in the backscattering configuration. It is known that backscattered light coming from the first scattering event can reveal the distribution of the scatterers' positions. The laser beam was focused through a lens of +62.9 mm focal length in order to obtain a parallel beam at the focus with its waist (~6.1 μm diameter) located on the sample's input surface. The backscattered light was collected perpendicular to the sample's surface by a CCD positioned at 65 mm from the surface. The incidence angle was ~45° regarding to the normal, which correspond to an incidence angle inside the sample of ~26°. In order to obtain a meaningful statistic and average the speckle pattern, a total of 400 images were recorded for each sample. Thus, to obtain the diffraction pattern produced by each RL system, the Fourier transform (FT) was determined separately for each of the 400 images, and then the mean FT was extracted. Afterwards, the diffraction pattern is obtained by the FT of this mean FT. The collection time for each image was 70 μs. For the experimental setup, see our recent work [14]. Note that the particles in the colloidal suspension are continuously moving, so, a short collection time is required. The FT is a workaround for the continuously changing diffraction pattern, because for small changes in the scatterers' position the FT is approximately the same. Note that the output of the FT represents the image in the frequency domain, thus, even if the particles move, the strong interaction between the particles would tend to preserve the separation between them and their structure. Thereby, the FT of the mean FT represents the average structure of the first layers of the colloid.

3. Results and discussion

3.1. Structural and morphological characterization

Fig. 1 shows the TEM image of the core–shell TiO_2@SiO_2–SiO_2 NPs. In the TEM image, the silica coating on the TiO_2 NPs shows a regular morphology, with a thickness of around 70–80 nm. Additionally, an appreciable amount of silica NPs with size of 40–50 nm are also synthesized during the TEOS hydrolysis, which can be observed in the TEM image. In order to determine the silica fraction in TiO_2@SiO_2–SiO_2 NPs, the suspension was precipitated by centrifuging and the atomic percentage ratios (Ti/Si) of the dried powders was studied by ED-XRF before and after centrifugation, yielding Ti_{51}/Si_{49} and Ti_{56}/Si_{44}, respectively, showing that the silica NPs represent 6.2 % in mass and 13 % in volume of the powder. The atomic percentage ratios (Ti/Si) for the TiO_2@SiO_2 powder was Ti_{70}/Si_{30}. The average silica shell thickness can be estimated considering the typical density of the silica obtained by the TEOS hydrolysis as being ~2.1 g cm^{-3}, which yields ~40 nm and ~70 nm thicknesses for TiO_2@SiO_2 and TiO_2@SiO_2–SiO_2, respectively. The hydrodynamic diameter D_{Hyd}, measured by DLS after precipitation by centrifuging, is appreciably larger for the TiO_2@SiO_2–SiO_2 NPs (D_{hyd} = 1450 nm) when compared to TiO_2@SiO_2 (D_{hyd} = 890 nm).

3.2. Random laser behavior

For a comparative study of the RL action in the TiO_2@SiO_2 and TiO_2@SiO_2–SiO_2 systems, RL emission was collected from the front (frontal collection) and the back (back collection) of the cuvette. For both RL systems, Fig. 2a shows the behavior of the emitted intensity (frontal collection) as a function of the pumping energy fluence. Emission spectra can be found in Figs. S1b–e of the supplementary materials. From Fig. 2a, we can observe that the RL efficiencies (RL_{eff}) for both systems are not constant. For the TiO_2@SiO_2 RL system (black squares), RL_{eff} decreases for pumping fluencies from ~15 mJ cm^{-2} up to ~35 mJ cm^{-2}. For pumping fluencies from >35 mJ cm^{-2} up to ~75 mJ cm^{-2}, RL_{eff} is again constant (magenta dotted line) and for pumping fluencies >75 mJ cm^{-2}, a complete saturation of the emission is observed. For the TiO_2@SiO_2–SiO_2 RL (red circles), RL_{eff} decreases for pumping fluencies from ~20 mJ cm^{-2} up to ~50 mJ cm^{-2}, where RL_{eff} starts to be again constant (magenta dotted line). A complete saturation of the emission is observed above ~110 mJ cm^{-2}. For both RL systems, the green dotted lines represent the RL_{eff} for fluencies below ~15 mJ cm^{-2}. For the TiO_2@SiO_2–SiO_2 RL system, RL_{eff} (<15 mJ cm^{-2}) is ~25 % higher than for the TiO_2@SiO_2 RL. Additionally, the saturated RL emission intensity is also around 25 % higher than for the TiO_2@SiO_2 system. The second slope efficiency for the TiO_2@SiO_2–SiO_2 system, RL_{eff} (pumping fluencies >50 mJ cm^{-2} and <110 mJ cm^{-2}), is ~70 % lower than that of the TiO_2@SiO_2 system (pumping fluencies >35 mJ cm^{-2} and <75 mJ

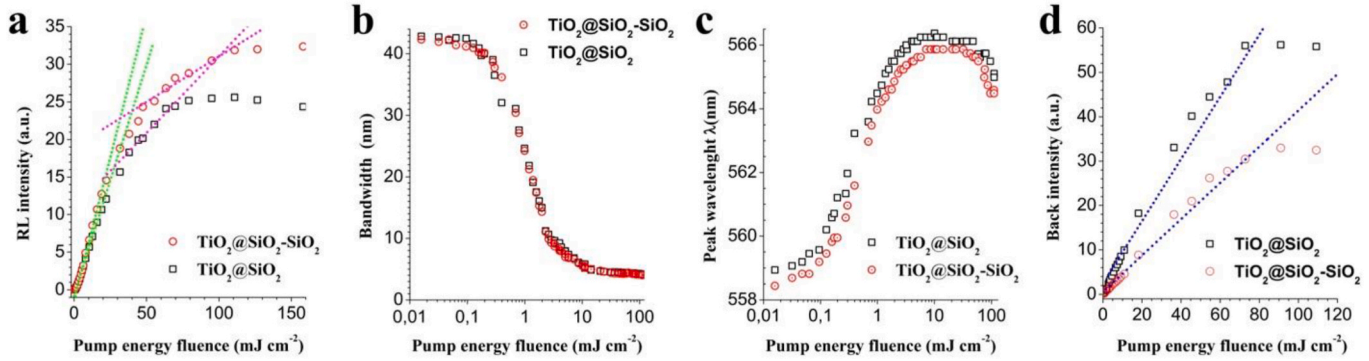

Fig. 2. For TiO_2@SiO_2–SiO_2 (red circles) and TiO_2@SiO_2 (black squares), influence of the pumping fluence on (a) the RL emitted peak intensity, RL_{eff}, for fluencies <15 mJ cm^{-2} (green dotted lines), the magenta dotted lines are RL_{eff} for fluencies >50 & <110 mJ cm^{-2} (TiO_2@SiO_2–SiO_2) and >35 & <75 mJ cm^{-2} (TiO_2@SiO_2), (b) RL spectral width (FWHM), (c) the peak position of the emission spectrum and d) emitted peak intensity for back collection, RL_{eff} (blue dotted lines), for fluencies <90 mJ cm^{-2} (TiO_2@SiO_2–SiO_2) and <70 mJ cm^2(TiO_2@SiO_2).

cm^{-2}). In our previous random lasing work in the TiO_2@SiO_2 system [7], we showed that the RL_{eff} for lower fluencies (<15 mJ cm^{-2}, green dotted lines) is basically associated to the emission of localized states. Therefore, the above results would indicate a stronger localization (higher density of localized states) for the TiO_2@SiO_2–SiO_2 RL system. For pumping fluencies >75 mJ cm^{-2} (TiO_2@SiO_2 system) and >110 mJ cm^{-2} (TiO_2@SiO_2–SiO_2 system), where the RL emission is saturated, a cavitation effect (bubbles emerging) starts to be observed. This phenomenon (higher fluencies) is reported for the first time in this TiO_2@Silica system, since in our previous work [7], random lasing was studied only for pumping fluencies <70 mJ cm^{-2}. We point out that the pumping fluence for emission saturation of the TiO_2@SiO_2–SiO_2 RL system is ~70 % higher than that of the TiO_2@SiO_2 RL system, which should be associated to stronger localization in the TiO_2@SiO_2–SiO_2 RL system. This latter result could indicate that the pressure exerted by trapped light inside localized states does not provoke an appreciable cavitation effect, which could be due to the "rigid" structure formed by the scatterers (their positions being strongly correlated) as consequence of the strong bond between them. If localized states are a result of the strong correlation in the scatterers' position [14,22], then, the pressure induced by trapped light in localized states should be rather propagated by this "rigid" structure and much less propagated in the liquid solution. Additionally, owing to the strong bond between scatterers, the amplitude of the mechanic wave, induced by the laser pulse and propagated through the colloidal structure, must decrease and its speed increase, causing a decrease in the pressure exerted on the liquid solution. Clearly, an increase in pumping fluence must provoke an increase of the pressure induced by trapped light, which can lead to a breakdown of the electrical bond between scatterers (Coulomb interactions) and, thus, the colloidal-ordered structure would be destroyed. This latter would favor the cavitation effect due to the propagation of photoacoustic wave through the liquid (ethanol). Fig. 2b shows the behavior of the spectral width (full width at half-maximum (FWHM)) for both RL systems as a function of the pumping energy fluence. Similar bandwidth narrowing (FWHM from ~45 nm down to ~5 nm) is observed for both RL systems when the pumping fluence is increased, from which it can be estimated that the RL threshold for both RL systems is almost identical (~1.2 mJ cm^{-2}).

For both RL systems, the RL emission peak (Fig. 2c) shows a redshift that increases rapidly for fluencies from ~0.08 up to ~8 mJ cm^{-2}. For fluencies between 8 and ~35 mJ cm^{-2}, the redshift is approximately constant for the TiO_2@SiO_2 system, which coincides with the starting decrease of RL_{eff} (Fig. 2a, black squares). For this system, the redshift starts to decrease for pumping fluencies >35 mJ cm^{-2}, at which the RL_{eff} starts again to be constant (<75 mJ cm^{-2}). For the TiO_2@SiO_2–SiO_2 RL system, the redshift is approximately constant for fluencies between 8 and ~50 mJ cm^{-2} and it starts to decrease for fluencies >50 mJ cm^{-2} (RL_{eff} starts to be constant at less than 110 mJ cm^{-2}). For both RL systems, the maximum redshift value (~7.6 nm) is large when compared with the customary maximum redshift for a TiO_2 NP system, which is around 3–4 nm. For comparison, the TiO_2@SiO_2 system at low [NPs] (diffusive regime) showed a maximum redshift of less than 1 nm [15,16]. For both RL systems (TiO_2@SiO_2–SiO_2 & TiO_2@SiO_2), the wavelengths of the RL emission peak below the RL threshold (fluorescence) is considerably lower (~558 nm) than for the TiO_2 NPs system and TiO_2@Silica system in the diffusive regime (~564 nm) [15]. This fact can be explained in the following way: The redshift was previously explained by a model considering absorption and emission at the transition between the ground state and the first excited singlet state of the dye molecule [46,47]. Polarization of R6G molecules below the population inversion threshold, induced by pump photons trapped within the localized states, should give rise to a photon-molecule bound state, due to the strong correlation of such photons [27,48]. After some time (residence time of the pump photons), the quantum state of the localized states changes due to thermal and/or nonlinear effects [7,49] giving rise to the emission of strongly correlated photons (fluorescence), which would propagate being poorly absorbed. Therefore, an emission band with shorter wavelengths is observed when compared with the TiO_2@-Silica system in the diffusive regime. We remark that for the TiO_2@-SiO_2–SiO_2 RL, the wavelength of RL emission peaks are ~0.5–0.7 nm lower than that of the TiO_2@SiO_2 RL system, which would indicate a stronger correlation of the emitted photons, i.e. higher density of localized states (stronger localization). As we previously demonstrated [7], RL emission of the TiO_2@SiO_2 system, collected frontally, is the result of overlapping localized and extended modes. In order to estimate the contribution of the RL modes, the extended modes (super fluorescence band or ASE) and the localized modes, the RL emission was also collected from the back of the cuvette (back-collection). Note that the emission of localized modes should basically be backscattered since they are very near the front surface [7], and too far from the back surface to survive, as the attenuation is huge. The back-collected spectra consisted of a broad emission band (~ 50 nm bandwidth) with an overlapped single emission band (see supplementary materials), whose intensity and bandwidth are dependent on the pumping energy [7]. This single emission band represents the emission of extended modes or ASE (see our previous work) [7]. Fig. 2d shows the behavior of the RL intensity, collected from the back of the cuvette (back-collection), as a function of the pumping fluencies. For the TiO_2@SiO_2 and TiO_2@SiO_2–SiO_2 RL systems, RL_{eff} (back-collection) were constant up to pumping fluencies of ~70 and ~90 mJ cm^{-2}, respectively. These saturation pumping fluencies (back-collection) are lower than those observed by frontal-collection. This latter can be explained by frontal emission being the contribution of both RL (localized and extended) modes, however, back emission is only from extended modes. In addition, the saturation

emission intensity and RL_{eff} (back-collection) for the $TiO_2@SiO_2$–SiO_2 RL are ~70 % lower than for the $TiO_2@SiO_2$ RL, which corresponds to the relationship between the efficiencies of the second slope in the frontal collection (Fig. 1a, magenta dotted lines). The latter shows that the RL emission in back-collection and the efficiency of the second slope in the frontal collection represent the emission of extended modes, which was shown in our previous work [7]. This fact corroborates our hypothesis that the frontal RL emission of the $TiO_2@SiO_2$–SiO_2 RL system presents higher contribution of localized modes and consequently a smaller contribution of extended modes. The above RL results were attributed to stronger localization of light (higher density of localized states) in the $TiO_2@SiO_2$–SiO_2 RL system when compared to the $TiO_2@SiO_2$ RL. This latter could be induced by stronger correlation in the scatterers' position due to stronger and longer-range interaction between $TiO_2@SiO_2$–SiO_2 NPs (larger D_{Hyd} & λ_{Debye}) [14]. In order to evaluate this hypothesis, comparative measurements of the transmittance and the light-diffraction were performed on both $TiO_2@SiO_2$–SiO_2 and $TiO_2@SiO_2$ RL systems.

3.3. Transmission measurements

For the $TiO_2@SiO_2$ and $TiO_2@SiO_2$–SiO_2 RL systems, the intensity profile of a Gaussian probe beam (He–Ne laser) was collected after propagating a distance $d \approx 1.8$ mm through the samples. In order to determine the transmittance, the integrated intensity profiles $I = \int I(x, y)\partial x\partial y = 2\pi \int I(r)\partial r$ were determined for both RL systems, where r is the radial distance from the beam center. Note that for the probe beam wavelength (633 nm), the R6G absorption is absolutely negligible when compared to the TiO_2@Silica absorption [3]. The relative transmittance $G = \frac{I_{(SiO2)}}{I_{(SiO2-SiO2)}}$ was determined, where $I_{(SiO2)}$ and $I_{(SiO2-SiO2)}$ are integrated transmitted intensities for the $TiO_2@SiO_2$ and $TiO_2@SiO_2$–SiO_2 RL systems, respectively. The relative transmittance G obtained from the transmission measurements was 1.78 ± 0.02, which indicates an appreciable decrease of transmittance for the $TiO_2@SiO_2$–SiO_2 RL system. This latter must be due to a conductance decrease and/or an absorption increase caused by the stronger light-matter coupling [3,14]. Both effects can be explained by a stronger localization (higher density of localized states), which in turn, would be caused by a stronger correlation in the scatterers' position ($TiO_2@SiO_2$–SiO_2) due to a longer-range Coulomb interaction (bigger D_{hyd} & λ_{Debye}). In order to confirm this hypothesis, measurements of the correlation in the scatterers' position in both, $TiO_2@SiO_2$–SiO_2 and $TiO_2@SiO_2$, RL systems were performed.

3.4. Measurements of the diffraction pattern from backscattered light

We proposed that lower transmittance of the $TiO_2@SiO_2$–SiO_2 RL system is a consequence of stronger localization, which in turn, is induced by a stronger correlation in the scatterers' position due to a stronger and longer-range interaction (Coulomb) between scatterers. This latter would be a consequence of a bigger D_{hyd} and λ_{Debye}, due to the thicker silica shell thickness. In order to get evidence that supports our hypothesis, we studied the diffraction patterns originated by both $TiO_2@SiO_2$ and $TiO_2@SiO_2$–SiO_2 RL systems when collecting the backscattered light perpendicular to the sample surface.

Fig. 3a and b shows the diffraction patterns obtained for the $TiO_2@SiO_2$–SiO_2 and $TiO_2@SiO_2$ RL systems, respectively. For both RL systems, a diffraction pattern with a hexagonal structure at the center can be observed, being better defined for the $TiO_2@SiO_2$–SiO_2 RL system. For the $TiO_2@SiO_2$–SiO_2 RL system, the diffraction maxima are smaller and there is less overlapping between them. The diffraction pattern seems to be proper of a cubic structure oriented in the (111) direction. This cubic structure with the plane (111) perpendicular to the sample surface represents a close packed structure of minor surface energy. Note that these RL suspensions are contained within a cuvette composed by two optical flats (fused silica), which should exert an additional repulsive force on the TiO_2@Silica NPs (scatterers) nearest to the surface. The latter must favor a close packing and ordering of the scatterers in the perpendicular direction and close to the surface (stronger correlation in the scatterers' position nearer to the surface). We remark that in our recently published work [14], for the same $TiO_2@SiO_2$ ethanol suspensions at FF<1 %, no diffraction patterns were observed, which indicated a homogeneous random medium (no correlation in the scatterers' positions). Additionally, we point out that the diffraction pattern obtained in this work for the same $TiO_2@SiO_2$ ethanol suspension ($FF = 4.8$ %) presents higher diffraction orders than that obtained in our recently published work [14]. We attribute the

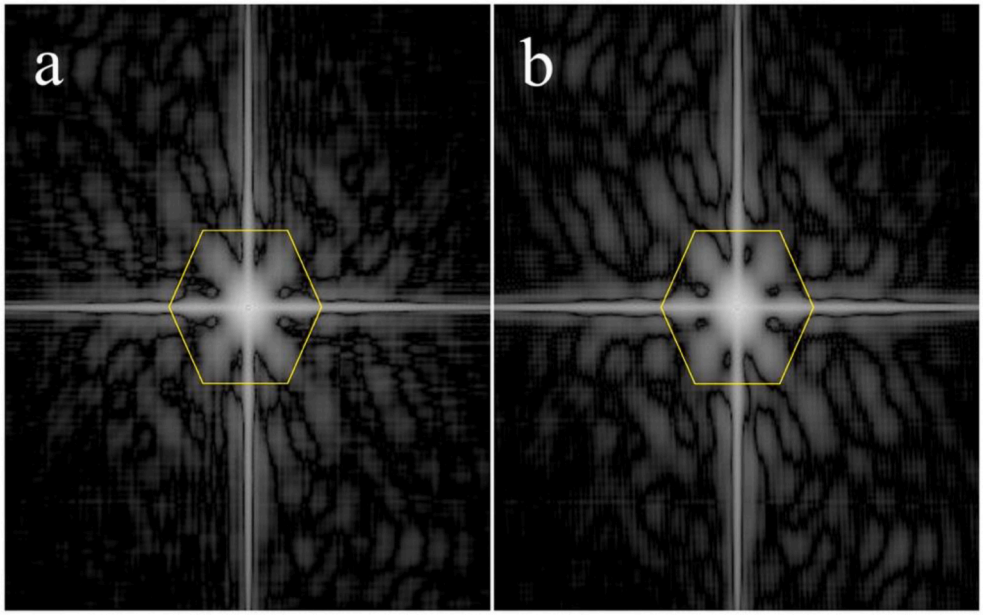

Fig. 3. Diffracted light collected in backscattering configuration for both RL systems ($TiO_2@SiO_2$–SiO_2 & $TiO_2@SiO_2$). The diffraction pattern (hexagonal structure) obtained from the $TiO_2@SiO_2$–SiO_2 RL system a) is better defined than the $TiO_2@SiO_2$–SiO_2 RL system b). The hexagonal structure outlined with a yellow line is observed at the central zone of the diffraction patterns.

latter to the larger irradiation area used in the present work (~6.1 μm diameter) when compared to the one used in our recent work (~4.4 μm dimeter) [14]. Thus, diffracted light coming from higher number of ordered NPs of TiO_2@SiO_2. Note that the number of diffraction orders must be sensitive to the irradiation area, since for this *FF* of 4.8 % the mean separation between particles in this structure (~1.3 μm) is of the order of the irradiation diameter (see our recent work) [14].

4. Conclusion

TiO_2 NPs coated with a thicker silica shell (~70 nm thickness, TiO_2@SiO_2–SiO_2), dispersed in ethanol, present a bigger hydrodynamic diameter (D_{Hyd} = 1450 nm) when compared to a thinner silica shell (~40 nm thickness, TiO_2@SiO_2, D_{Hyd} = 890 nm) used in our previous works [3,5,7,14]. Light diffraction experiments demonstrated a stronger correlation in the scatterers' position for the TiO_2@SiO_2–SiO_2 RL system (thicker silica shell), which we associated to the longer-range of Coulomb interaction between TiO_2@SiO_2–SiO_2 NPs (larger D_{Hyd} & λ_{Debye}). Transmission measurement in the TiO_2@SiO_2–SiO_2 RL system showed a transmittance ~1.8 times lower than the TiO_2@SiO_2 RL system, which indicates a conductance decrease and/or an absorption increase when compared to the TiO_2@SiO_2 RL system. This latter was attributed to a stronger localization (higher density of localized states). Notice that both systems are composed by suspensions of particles with the same concentrations and with similar optical scattering strength. Thus, owing to "*correlation-induced localization*" [22] [–] [24] a stronger correlation in the scatterers' position leads to stronger localization, and consequently, lower conductance and stronger enhancement of the light-matter coupling (higher absorption) [14]. The TiO_2@SiO_2–SiO_2 RL system (front-collection) presented an RL_{eff} (pumping fluencies <15 mJ cm^{-2}) and a saturated RL emission intensity 25 % higher than the TiO_2@SiO_2 RL system. In addition, the pumping fluence for saturation of the RL emission and the seeming cavitation effect was ~70 % higher for the TiO_2@SiO_2–SiO_2 RL system when compared to the TiO_2@SiO_2 RL. This latter suggests that the pressure exerted by the pumping light trapped in localized states does not propagate appreciably within the liquid solution due to the "rigid structure" formed by the strongly bounded scatterers. Therefore, this phenomenon could allow the generation of mechanical waves by resonating these colloidal structures. A photo-acoustic study as a function of the crystallization (increasing correlation in the scatterers' position) of this colloidal structure is called for, in order to confirm our hypothesis. The RL emission (back--collection), which allowed the separate measurement of the RL extended modes, showed that the RL_{eff} (back-collection) of the TiO_2@SiO_2 RL system was ~70 % higher than in the TiO_2@SiO_2–SiO_2 RL system, which corresponds to the relationship observed between the second slope efficiencies in the frontal collection. These RL measurements (front and back collections) demonstrated a higher contribution of RL localized modes for the TiO_2@SiO_2–SiO_2 RL system when compared to the TiO_2@SiO_2 RL system. In short, we showed that core-shell TiO_2@Silica NPs in ethanol solution with a thicker silica shell (TiO_2@SiO_2–SiO_2 NPs) presents larger D_{Hyd} and λ_{Debye}, which implies longer-range Coulomb interaction between NPs (scatterers). This latter causes stronger correlation in the scatterers' position, demonstrated by the light diffraction experiment, which induces stronger localization and associated phenomena (random lasing).

Author contribution

C.T.D., A.A.V.G., V.M. & E.J.V. synthesized nanoparticles and prepared samples, N.W., J.D. & E.J.V. performed TEM, DLS and ED-XRF characterization, C.T.D., A.A.V.G., W.S.M. & E.J.V. performed the transmission and diffraction experiments, C.T.D., A.A.V.G., V.M., N.W., J.D. & E.J.V. performed random lasing experiments, C.T.D., A.A.V.G., V. M., N.W., W.S.M. & E.J.V. analyzed and discussed the results and E.J.V. wrote the manuscript and guided the research.

Author agreement

The manuscript has been read and approved by all listed authors. None of the material contained within the manuscript has been or is under consideration for publication elsewhere.

Declaration of competing interest

The authors declare that they have no known competing financial interests or personal relationships that could have appeared to influence the work reported in this paper.

Acknowledgements

We gratefully acknowledge financial support from FAPESP (grants 2017/05854-9 and 2017/10765-5) and CAPES. We appreciate useful experimental support of Professors Mario Ugulino and Paulo C. Oliveira.

Appendix A. Supplementary data

Supplementary data to this article can be found online at https://doi.org/10.1016/j.optmat.2021.111428.

References

[1] P. Allende, L. Barrientos, A. Orera, M.A. Laguna-Bercero, N. Salazar, M. L. Valenzuela, C. Diaz, TiO2/SiO2 composite for efficient protection of UVA and UVB rays through of a solvent-less synthesis, J. Cluster Sci. 30 (6) (2019) 1511–1517.

[2] X. Feng, S. Zhang, X. Lou, Controlling silica coating thickness on TiO2 nanoparticles for effective photodynamic therapy, Colloids Surf. B Biointerfaces 107 (2013) 220–226.

[3] E. Jimenez-Villar, I.F. Da Silva, V. Mestre, P.C. De Oliveira, W.M. Faustino, G.F. De Sá, Anderson localization of light in a colloidal suspension (TiO2@silica), Nanoscale 8 (21) (2016) 10938–10946.

[4] E. Jimenez-Villar, M.C.S. Xavier, N.U. Wetter, V. Mestre, W.S. Martins, G.F. Basso, V.A. Ermakov, F.C. Marques, G.F. de Sá, Anomalous transport of light at the phase transition to localization: strong dependence with incident angle, Photon. Res. 6 (10) (2018) 929–942, https://doi.org/10.1364/PRJ.6.000929.

[5] E. Jimenez Villar, M.C.S. Xavier, J.G.G.S. Ramos, N.U. Wetter, V. Mestre, W. S. Martins, G.F. Basso, V.A. Ermakov, F.C. Marques, G.F. de Sá, Localization of Light: Beginning of a New Optics, in: D.L. Andrews, E.J. Galvez, J. Glückstad (Eds.), Complex light and Optical Forces XII 10549, Proceeding SPIE, 2018, p. 1054905.

[6] E. Jimenez-Villar, V. Mestre, N.U. Wetter, G. F de Sá, Core-shell (TiO2@Silica) Nanoparticles for Random Lasers, in: D.L. Andrews, E.J. Galvez, J. Glückstad (Eds.), Complex light and Optical Forces XII 10549, Proceeding SPIE, 2018, p. 105490D.

[7] E. Jiménez-Villar, I.F. da Silva, V. Mestre, N.U. Wetter, C. Lopez, P.C. de Oliveira, W.M. Faustino, G.F. de Sá, Random lasing at localization transition in a colloidal suspension (TiO2@Silica), ACS Omega 2 (6) (2017) 2415–2421.

[8] N. Wetter, E. Jimenez-Villar, Random laser materials: from ultrahigh efficiency to very low threshold (Anderson localization), J. Mater. Sci. Mater. Electron. 30 (18) (2019) 16761–16773.

[9] N.U. Wetter, J.M. Giehl, F. Butzbach, D. Anacleto, E. Jiménez-Villar, Polydispersed powders (Nd 3+ :YVO 4) for ultra efficient random lasers, Part. Part. Syst. Char. 35 (4) (2018) 1700335.

[10] N.U. Wetter, A. Ramos de Miranda, É. Pecoraro, S.J. Lima Ribeiro, E. Jimenez-Villar, Dynamic random lasing in silica aerogel doped with rhodamine 6G, RSC Adv. 8 (52) (2018) 29678–29685.

[11] Z. Wang, M. Fan, H. Wu, Y. Li, Y. Li, L. Zhang, Y. Rao, Cascaded random distributed-feedback Raman fiber laser assisted by Fresnel reflection, Opt Express 23 (21) (2015) 28076.

[12] Z. Ren, N. Zheng, K. Ge, G. Zhang, S. Li, Investigation of the LSPR on a wavelength-tunable random laser, Phys. Scripta 94 (10) (2019) 105501.

[13] K.C. Jorge, M.A. Alvarado, E.G. Melo, M.N.P. Carreño, M.I. Alayo, N.U. Wetter, Directional random laser source consisting of a HC-ARROW reservoir connected to channels for spectroscopic analysis in microfluidic devices, Appl. Opt. 55 (20) (2016) 5393.

[14] V.A. Ermakov, W.S. Martins, N.U. Wetter, F.C. Marques, E. Jiménez-Villar, Localization of light induced in ordered colloidal suspensions: powerful sensing tools, Nanoscale 13 (13) (2021) 6417–6425, https://doi.org/10.1039/D0NR08736J.

[15] E. Jimenez-Villar, V. Mestre, P.C. de Oliveira, G.F. de Sá, Novel core–shell (TiO2@Silica) nanoparticles for scattering medium in a random laser: higher efficiency, lower laser threshold and lower photodegradation, Nanoscale 5 (24) (2013) 12512.

[16] E. Jimenez-Villar, V. Mestre, P.C. de Oliveira, W.M. Faustino, D.S. Silva, G.F. de Sá, TiO 2 @Silica nanoparticles in a random laser: strong relationship of silica shell

thickness on scattering medium properties and random laser performance, Appl. Phys. Lett. 104 (8) (2014), 081909.
[17] G. Fuertes, O.L. Sánchez-Muñoz, E. Pedrueza, K. Abderrafi, J. Salgado, E. Jiménez, Switchable bactericidal effects from novel silica-coated silver nanoparticles mediated by light irradiation, Langmuir 27 (6) (2011) 2826–2833.
[18] E. Jiménez, K. Abderrafi, R. Abargues, J.L. Valdés, J.P. Martínez-Pastor, Laser-Ablation-induced synthesis of SiO 2 -capped noble metal nanoparticles in a single step, Langmuir 26 (10) (2010) 7458–7463.
[19] G. Fuertes, E. Pedrueza, K. Abderrafi, R. Abargues, O. Sánchez, J. Martínez-Pastor, J. Salgado, E. Jiménez, Photoswitchable Bactericidal Effects from Novel Silica-Coated Silver Nanoparticles, in: R. Sroka, L.D. Lilge (Eds.), Progress in Biomedical Optica and Imaging 8092, Proceeding SPIE, 2011, p. 80921M.
[20] V.A. Ermakov, E. Jimenez-Villar, J.M.C. da Silva Filho, E. Yassitepe, N.V.V. Mogili, F. Iikawa, G.F. de Sá, C.L. Cesar, F.C. Marques, Size control of silver-core/silica-shell nanoparticles fabricated by laser-ablation-assisted chemical reduction, Langmuir 33 (9) (2017) 2257–2262.
[21] J.R. González-Castillo, E. Rodríguez-González, E. Jiménez-Villar, C.L. Cesar, J. A. Andrade-Arvizu, Assisted laser ablation: silver/gold nanostructures coated with silica, Appl. Nanosci. 7 (8) (2017) 597–605.
[22] P.A. Nosov, I.M. Khaymovich, V.E. Kravtsov, Correlation-induced localization, Phys. Rev. B 99 (10) (2019), 104203.
[23] R. Wang, M. Röntgen, C.V. Morfonios, F.A. Pinheiro, P. Schmelcher, L.D. Negro, Edge modes of scattering chains with aperiodic order, Opt. Lett. 43 (9) (2018) 1986–1989.
[24] F. Sgrignuoli, R. Wang, F.A. Pinheiro, L. Dal Negro, Localization of scattering resonances in aperiodic Vogel spirals, Phys. Rev. B 99 (10) (2019), 104202.
[25] S. John, Electromagnetic absorption in a disordered medium near a photon mobility edge, Phys. Rev. Lett. 53 (22) (1984) 2169–2172.
[26] S. John, Strong localization of photons in certain disordered dielectric superlattices, Phys. Rev. Lett. 58 (23) (1987) 2486–2489.
[27] S. John, J. Wang, Quantum electrodynamics near a photonic band gap: photon bound states and dressed atoms, Phys. Rev. Lett. 64 (20) (1990) 2418–2421.
[28] S. John, J. Wang, Quantum optics of localized light in a photonic band gap, Phys. Rev. B 43 (16) (1991) 12772–12789.
[29] E. Yablonovitch, Inhibited spontaneous emission in solid-state physics and electronics, Phys. Rev. Lett. 58 (20) (1987) 2059–2062.
[30] D.S. Wiersma, P. Bartolini, A. Lagendijk, R. Righini, Localization of light in a disordered medium, Nature 390 (6661) (1997) 671–673.
[31] M. Störzer, P. Gross, C.M. Aegerter, G. Maret, Observation of the critical regime near anderson localization of light, Phys. Rev. Lett. 96 (6) (2006) 1–4.
[32] T. Sperling, W. Bührer, C.M. Aegerter, G. Maret, Direct determination of the transition to localization of light in three dimensions, Nat. Photonics 7 (1) (2013) 48–52.
[33] F. Scheffold, R. Lenke, R. Tweer, G. Maret, Localization or classical diffusion of light? Nature 398 (6724) (1999) 206–207.
[34] F. Scheffold, D. Wiersma, Inelastic scattering puts in question recent claims of Anderson localization of light, Nat. Photonics 7 (12) (2013) 934.
[35] T. Van Der Beek, P. Barthelemy, P.M. Johnson, D.S. Wiersma, A. Lagendijk, Light transport through disordered layers of dense gallium arsenide submicron particles," Phys. Rev. B - Condens, Matter Mater. Phys. 85 (11) (2012) 1–11.
[36] T. Sperling, L. Schertel, M. Ackermann, G.J. Aubry, C.M. Aegerter, G. Maret, Can 3D light localization be reached in "white paint"? New J. Phys. 18 (1) (2016) 13039.
[37] S.E. Skipetrov, I.M. Sokolov, Absence of anderson localization of light in a random ensemble of point scatterers, Phys. Rev. Lett. 112 (2) (2014), 023905.
[38] R.J. Hunter, in: Foundations of Colloid Science, second ed., Oxfort University press,, 2001.
[39] O.L. Sánchez-Muñoz, J. Salgado, J. Martínez-Pastor, E. Jiménez-Villar, Synthesis and physical stability of novel Au-Ag@SiO2 alloy nanoparticles, Nanosci. Nanotechnol. 2 (1) (2012) 1–7.
[40] D. Bastos, F.J. de las Nieves, "Colloidal stability of sulfonated polystyrene model colloids. Correlation with electrokinetic data,", Colloid Polym. Sci. 272 (5) (1994) 592–597.
[41] L. Bressel, R. Hass, O. Reich, Particle sizing in highly turbid dispersions by Photon Density Wave spectroscopy, J. Quant. Spectrosc. Radiat. Transf. 126 (2013) 122–129.
[42] S. Mujumdar, M. Ricci, R. Torre, D.S. Wiersma, Amplified extended modes in random lasers, Phys. Rev. Lett. 93 (5) (2004), 053903.
[43] H.E. Tureci, L. Ge, S. Rotter, A.D. Stone, Strong interactions in multimode random lasers, Science (80-.) 320 (5876) (2008) 643–646.
[44] O. Zaitsev, L. Deych, Recent developments in the theory of multimode random lasers, J. Opt. 12 (2) (2010), 024001.
[45] K. Abderrafi, E. Jiménez, T. Ben, S.I. Molina, R. Ibáñez, V. Chirvony, J.P. Martínez-Pastor, Production of nanometer-size GaAs nanocristals by nanosecond laser ablation in liquid, J. Nanosci. Nanotechnol. 12 (8) (2012) 6774–6778.
[46] M.A. Noginov, H.J. Caulfield, N.E. Noginova, P. Venkateswarlu, Line narrowing in the dye solution with scattering centers, Opt Commun. 118 (3–4) (1995) 430–437.
[47] C. Tolentino Dominguez, E. de Lima, P.C. de Oliveira, F. López Arbeloa, Using random laser emission to investigate the bonding energy of laser dye dimers, Chem. Phys. Lett. 464 (4–6) (2008) 245–248.
[48] S. John, Localization of light, Phys. Today 44 (5) (1991) 32.
[49] M. Büttiker, M. Moskalets, From anderson localization to mesoscopic physics, Int. J. Mod. Phys. B 24 (12n13) (2010) 1555–1576.